Molecular Crystals and Liquid Crystals

ISSN: 1542-1406 (Print) 1563-5287 (Online) Journal homepage: http://www.tandfonline.com/loi/gmcl20

Synthesis, characterization, single crystal X-ray diffraction and DFT studies of ethyl 5-methyl-1-phenyl-1H-pyrazole-4-carboxylate

S. Viveka, G. Vasantha, Dinesha, S. Naveen, N. K. Lokanath & G. K. Nagaraja

To cite this article: S. Viveka, G. Vasantha, Dinesha, S. Naveen, N. K. Lokanath & G. K. Nagaraja (2016) Synthesis, characterization, single crystal X-ray diffraction and DFT studies of ethyl 5-methyl-1-phenyl-1H-pyrazole-4-carboxylate, Molecular Crystals and Liquid Crystals, 629:1, 135-145, DOI: 10.1080/15421406.2015.1107813

To link to this article: http://dx.doi.org/10.1080/15421406.2015.1107813

MOLECULAR CRYSTALS AND LIQUID CRYSTALS
2016, VOL. 629, 135–145
http://dx.doi.org/10.1080/15421406.2015.1107813

Taylor & Francis
Taylor & Francis Group

Synthesis, characterization, single crystal X-ray diffraction and DFT studies of ethyl 5-methyl-1-phenyl-1H-pyrazole-4-carboxylate

S. Viveka[a], G. Vasantha[b], Dinesha[a], S. Naveen[c], N. K. Lokanath[d], and G. K. Nagaraja[a]

[a]Department of Studies in Chemistry, Mangalore University, Mangalagangothri, Mangalore, Karnataka, India;
[b]Chemistry of Interfaces, Division of Chemical Engineering, Luleå University of Technology, Luleå, Sweden;
[c]Institution of Excellence, Vijnana Bhavana, Manasagangotri, University of Mysore, Mysore, Karnataka, India;
[d]Department of Studies in Physics, Manasagangotri, University of Mysore, Mysore, Karnataka, India

ABSTRACT

The present study describes the synthesis, spectroscopic, and single crystal X-ray structural analysis of ethyl 5-methyl-1-phenyl-1H-pyrazole-4-carboxylate. The pyrazole ester of formula [$C_{13}H_{14}N_2O_2$] was prepared from the three-component one-pot condensation reaction of ethyl acetoacetate, N,N-dimethyldimethoxymethanamine, and phenyl hydrazine. The product was crystallized by using ethanol as solvent. The structure of the compound was confirmed by elemental analysis, Fourier transforms infrared (IR), thermogravimetric analysis, UV-visible (UV-Vis), ^{1}H NMR, and single-crystal X-ray diffraction studies. The gas-phase molecular geometry and the electronic structure-property of the molecule were calculated at the density functional theory. The frontier molecular orbitals, theoretical UV-Vis, and IR stretching vibrations were also reported. The compound crystallizes in the monoclinic system with the space group $P2_1/c$ and $Z = 4$. The unit cell parameters are a = 12.141(3) Å, b = 13.934(4) Å, c = 7.2777(18) Å, and $\beta = 97.816(14)^0$. The structure is stabilized by an intermolecular interaction of type C-H···O and the structure also involves C-H···π interactions.

KEYWORDS

Crystallization; crystal structure; DFT; FTIR spectrum; pyrazole; thermogram

1. Introduction

Pyrazole refers to the class of simple aromatic compounds of the heterocyclic series, characterized by a five-membered ring structure composing of three carbon atoms and two nitrogen atoms in adjacent positions. Pyrazoles and its derivatives, a class of well-known nitrogen heterocycles, occupy a prime position in medicinal and pesticide chemistry for their diverse biological activities. They have displayed a broad spectrum of pharmacological and biological activities such as anti-inflammatory, antibacterial, anticancer, antiviral, herbicidal, and insecticidal [1–7]. The pyrazole moiety is present as the core in some of the leading drugs such as celebrex, ionazlac, rimonabant, difenamizole, etc. [8]. The bioactivity of functionalized *N*-arylpyrazole was extensively studied and the C-5 substituted pyrazoles are also exploited in

CONTACT G. K. Nagaraja nagarajagk@gmail.com Department of Post Graduate Studies and Research in Chemistry, Mangalore University, Mangalagangothri 574 199 Mangalore Karnataka, India.
Color versions of one or more of the figures in the article can be found online at www.tandfonline.com/gmcl.

the design of pharmaceuticals and agrochemical agents [9,10]. In addition, the pyrazole analogues have also found use as building blocks in organic synthesis for designing pharmaceutical and agrochemicals [11]. The wide range of biological activities associated with pyrazole and its derivatives have made them popular synthetic targets. Recently, much attention has been paid to the design and synthesis of pyrazole derivatives [12,13]. Although, the organic chemists have devised a broad range of methods for the synthesis of pyrazoles and new methods continue to appear, the design of new pyrazole forming reactions is still a compelling research topic. Multicomponent reactions (MCR) have emerged as a powerful tool for delivering the molecular diversity needed in the combinatorial approaches for the preparation of bioactive heterocyclic compounds [14,15].

The computational approaches based on molecular orbital (MO) and density functional theory (DFT), which focuses on the total electron density of a molecule, can be used to describe the molecular structure and properties of molecules of interest whereby complementing the experimental results. The prediction of UV-visible (UV-Vis) spectrum and harmonic vibrational frequencies on the basis of DFT is of great help in the assignment of experimental results [16]. On the other hand, MO theory can assess reactivity in terms of frontier MOs (FMOs), in particular, the energy, atomic distribution, and symmetry of the highest occupied MO (HOMO) and lowest unoccupied MO (LUMO) [17].

In view of these observations, we have synthesized pyrazole ester ($C_{13}H_{14}N_2O_2$) by the MCR. The crystal structure is characterized by single-crystal X-ray diffraction, elemental analysis, UV-Vis spectra, Fourier transforms infrared (FTIR), and proton nuclear magnetic resonance (^{1}H NMR). The change in the mass of a substance, as a function of temperature when it is heated, is monitored using thermogravimetric analysis (TGA). Also, the variation of heat flow with temperature can be measured by using the differential scanning calorimetry (DSC). The DFT calculation is used in order to perform the structural analysis of the studied molecules. The presence of ester functionality in pyrazoles further offers an attractive method for the generation of derivatives which may possess interesting medicinal and biological properties.

2. Experimental

2.1. *Materials and methods*

All chemicals were purchased commercially and used without prior purification. IR spectra was recorded on a Shimadzu FTIR spectrophotometer in the range 400–4000 cm^{-1} using the KBr pellets. TGA and DSC measured using Perkin Elmer Thermal Analysis instrument and Netzsch instrument, respectively. The experiment was carried out in nitrogen atmosphere at a heating rate of 20 °C/min in the temperature range between 30 °C and 450 °C. The UV-Vis spectrum was recorded in Shimadzu UV-2550 UV-Vis spectrophotometer. Elemental analysis was carried out by using VARIO EL-III (Elementar 10 Analysensysteme GmBH). Melting points were determined in open capillary tube and were uncorrected. The ^{1}H NMR spectra was recorded on a Bruker AMX 400 NMR spectrometer with 5 mm PABBO BB-1H probe using dimethyl sulfoxide (DMSO-D6) as solvent. The X-ray intensity data were collected at a temperature of 293 K on a Bruker Proteum2 CCD diffractometer equipped with an X-ray generator operating at 45 kV and 10 mA, using Cu$K\alpha$ radiation of wavelength 1.54178 Å. Data were collected for 24 frames per set with different settings of φ (0° and 90°), keeping the scan width of 0.5°, exposure time of 2 sec, the sample to detector distance of 45.10 mm, and 2θ value at 46.6°. A complete data set was processed using SAINT PLUS [18]. The parameters

of the molecular geometry, electronic structure, and harmonic frequency calculations were calculated using Amsterdam Density Functional package (ADF 2014.01) [19,20]. In all our calculations, we have used generalized gradient approximation with Perdew-Burke-Ernzerhof (PBE) exchange-correlation functional [21]. The coordinates from the X-ray diffraction data were used as the starting structure for geometry optimization by DFT method. The geometry was fully optimized at the triple-ζ basis set with two sets of polarization functions (TZ2P) basis set level followed by the vibrational frequency calculations (no imaginary frequencies). FMOs were obtained at the same level of theory and plotted using the ADF view program.

2.2. *Synthesis of compound of ethyl 5-methyl-1-phenyl-1H-pyrazole-4-carboxylate*

The starting material, (*E*)-2-acetyl-3-(dimethylamino)-2-propenoate (**2**), was obtained via condensation of ethyl acetoacetate (**1**) with *N*,*N*-dimethyldimethoxymethanamine (DMF-DMA), which on cyclocondensation with phenyl hydrazine resulted in the target compound 5-methyl-1-phenyl-1H-4-pyrazolecarboxylate (**3**). The reaction scheme is explained in Scheme 1 [22]. Melting point 73°C–75°C. Elemental analysis for $C_{13}H_{14}N_2O_2$ (%): C (67.81); H (6.13); and N (12.17). Found: C (67.79); H (6.15); and N (12.15).

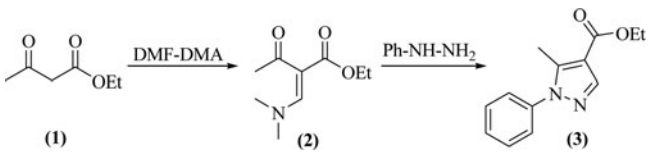

Scheme 1. Proposed reaction scheme for the formation of 5-methyl-1-phenyl-1H-4-pyrazolecarboxylate **(3)**.

3. Results and discussion

3.1. *UV-Vis spectral analysis*

Absorption of ultraviolet radiation by an organic molecule may lead to the electronic excitations among the various energy levels within the molecule. The UV-Vis spectrum was recorded by using dimethylformamide (DMF) as solvent (Fig. 1).

For the target compound **(3)**, it was observed that the compound shows an absorption peak at 266 nm, which could be attributed to the transition between nonbonding atomic orbitals holding unshared pair of electrons and antibonding pi-orbitals (C = O), i.e., n-$\pi*$ transitions. The calculated absorption values are 278, 274, 251, and 243 nm; however, the region below 250 nm is not seen in the experimental spectra. The first two are singlet-singlet excitations from HOMO (60%) and HOMO-1 (40%) to LUMO, where the percentage within parenthesis refers to major contributions to each of these excitations. On the other hand, the excitations at 251 and 243 nm have major contributions from HOMO-3, HOMO-2, and HOMO-1 to LUMO, LUMO+1, and LUMO+2. The discrepancy between the calculated and the experimental spectra is expected as the calculation was done at the gas-phase unlike the experiment, which was measured in DMF solution.

3.2. *Thermal analysis (DSC-TGA)*

The TGA and DSC curve, which emphasizes the thermal stability of the crystals are shown in Fig. 2.

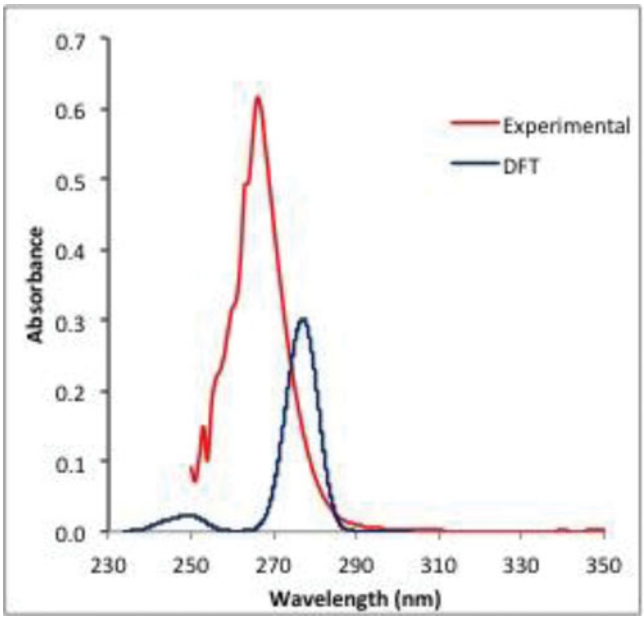

Figure 1. Theoretical and experimental UV-Vis spectra of the crystal.

Compound **(3)** exhibited the endothermal peak at 74.6 °C corresponds to the melting point of the crystal. It was found that the pure crystal starts to decompose in the range of temperature between 160 °C and 280 °C. The endothermic peaks at 271.5 °C also show the stage of decomposition.

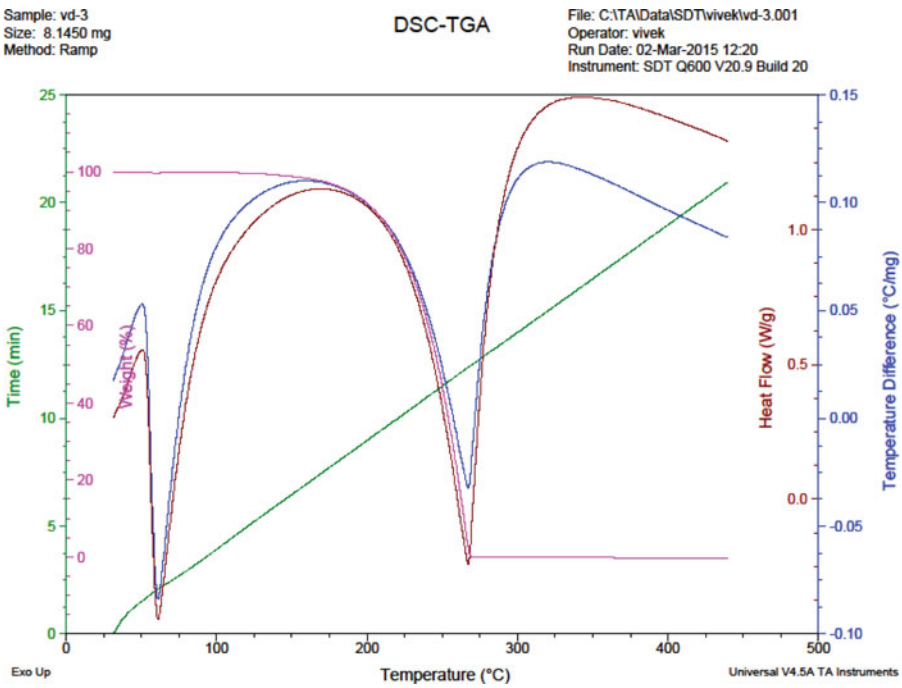

Figure 2. The DSC-TGA curves of pure 5-methyl-1-phenyl-1H-4-pyrazolecarboxylate crystal **(3)**.

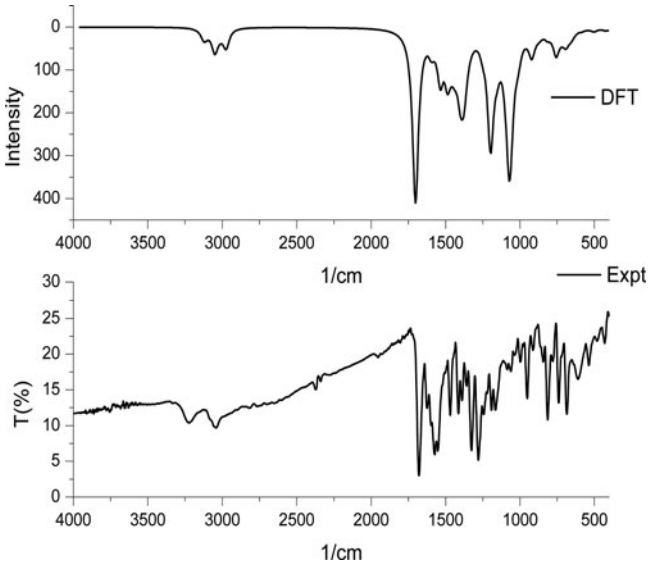

Figure 3. Theoretical and experimental FTIR spectra of 5-methyl-1-phenyl-1H-4- pyrazolecarboxylate crystal.

3.3. *FTIR spectral analysis*

The theoretical and experimental FTIR spectra of the crystal structure are shown in Fig. 3. As explained in Fig. 3, the IR spectrum can be used to identify the functional groups present in the molecule.

In an experimental result of FTIR spectrum, the ester functionality can be characterized by a strong C = O stretching frequency near 1680 cm^{-1}. Additionally, the C-O stretching bands in esters can also be highly informative. All esters exhibit strong C-O stretching absorption in the range of 1030–1300 cm^{-1}. In our case, the aryl ester exhibited two C-O stretching bands near 1278 and 1161 cm^{-1} which are due to the asymmetric and symmetric stretching. The weak absorptions at 3041 cm^{-1} could be attributed to the aromatic C-H stretching vibrations. Figure 3 shows the calculated IR spectrum of **(3)** at PBE/TZ2P level. Here, the peaks within the range of 2900–3200 cm^{-1} are attributed to the asymmetric stretching of aromatic, symmetric, and asymmetric stretching of pyrazole methyl protons (3123, 3052, and 2918, respectively) bond vibrations. The C = O stretching at 1702 cm^{-1} was very close to the experimental value.

Comparison of the vibrational frequencies calculated at PBE/TZ2P with experimental values reveals that PBE/TZ2P basis set gives reasonable deviations from the experimental values. These deviations between the calculated and experimental vibrational frequencies are due to the fact that the calculations were performed on a single molecule in the gaseous state unlike the experimental results, which was obtained for the powdered sample characterized by the intermolecular interactions. Also, the DFT calculated structure has slightly different geometry than the experimental one.

3.4. *^{1}H NMR spectral analysis*

The ^{1}H NMR spectra of compound **(3)** is shown in Fig. 4. The spectrum shows well resolved peaks for ethyl, methyl, and pyrazole protons where as the phenyl protons are severely

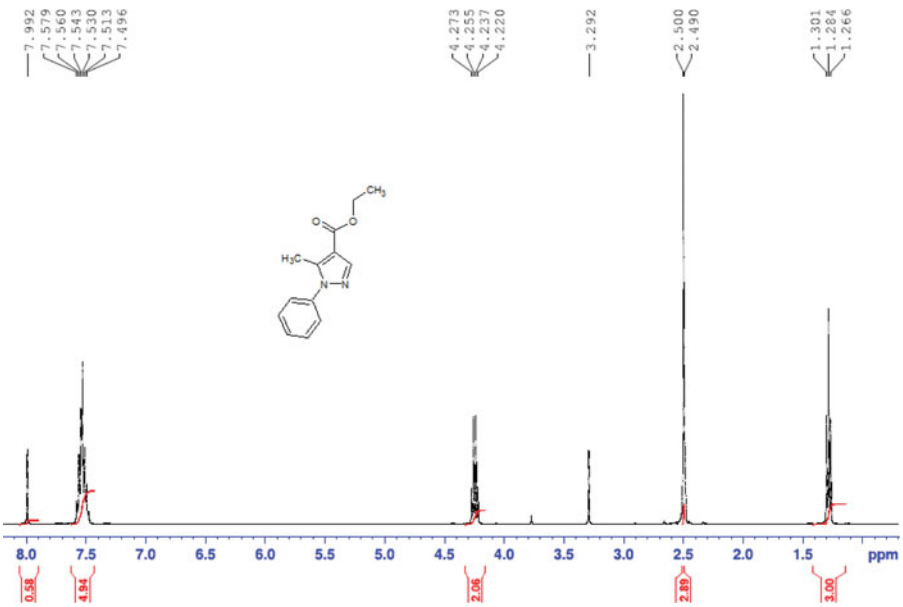

Figure 4. [1]H NMR spectra of 5-methyl-1-phenyl-1H-4-pyrazolecarboxylate (solution in DMSO).

overlapped. A triplet at $\delta = 1.26$ ppm and quartet at $\delta = 4.22$ ppm confirm the presence of methyl and methylene protons of the ester chain. The singlet at $\delta = 2.49$ ppm (overlapped with DMSO peak) could be assigned to the pyrazole methyl protons while the multiplets observed in the region $\delta = 7.49$–7.57 ppm to the five phenyl protons. The downfield shifted peak at $\delta = 7.99$ ppm was assigned to the pyrazole proton.

3.5. *Single crystal X-ray diffraction method*

A brown colored prismatic single crystal of dimensions $0.3 \times 0.27 \times 0.25$ mm^3 of the title compound was chosen for an X-ray diffraction study. The structure was solved by direct methods and refined by full-matrix least squares method on F^2 using SHELXS and SHELXL programs [23]. All the nonhydrogen atoms were revealed in the first difference Fourier map itself while the hydrogen atoms were positioned geometrically and were refined using a riding model. After 10 cycles of refinement, the final difference Fourier map showed peaks of no chemical significance and the residuals saturated to 0.0466. The geometrical calculations were carried out using the program PLATON [24]. The molecular and packing diagrams were generated using the software MERCURY [25]. The details of the crystal structure and data refinement are given in Table 1. The list of bond lengths and bond angles of the nonhydrogen atoms are given in Tables 2 and 3, respectively. Figure 5 represents the ORTEP diagram of the molecule with thermal ellipsoids drawn at 50% probability.

The molecule has adopted a nonplanar geometry with normal bond lengths and bond angles. The molecular conformation is characterized by a dihedral angle of 56.69(10)° between the mean planes of the two aromatic rings, which is lesser than the corresponding value of 64.05(13)°. The carbonyl group at C7 is oriented in an −antiperiplanar conformation as indicated by the torsion angle value of −174.18(17)° for O8-C7-C4-C5. The torsion angle values of −179.56(13)° and 173.86(16)° for C4-C7-O9-C10 and C7-O9-C10-C11,

Table 1. Crystal data and structure refinement table.

Parameter	Value
CCDC deposit No.	CCDC 105,4933
Empirical formula	$C_{13}H_{14}N_2O_2$
Formula weight	230.26
Temperature	293(2) K
Wavelength	1.54178 SÅ
Crystal system, space group	Monoclinic, $P2_1/c$
Unit cell dimensions	$a = 12.141(3)$ SÅ, $b = 13.934(4)$ SÅ, $c = 7.2777(18)$ SÅ
Volume	1219.8(5) SÅ^3
Z, Calculated density	4, 1.254 Mg/m^3
Absorption coefficient	0.699 mm^{-1}
$F_{(000)}$	488
Crystal size	0.3 × 0.27 × 0.25 mm^3
Theta range for data collection	6.91° to 64.31°
Limiting indices	$-14 \le h \le 13$, $-15 \le k \le 15$, $-7 \le l \le 8$
Reflections collected/unique	6755/1966 [R(int) = 0.0699]
Refinement method	Full-matrix least-squares on F^2
Data/restraints/parameters	1966/0/156
Goodness-of-fit on F^2	1.058
Final R indices [$I > 2\sigma(I)$]	$R1 = 0.0466$, $wR2 = 0.1410$
R indices (all data)	$R1 = 0.1036$, $wR2 = 0.1538$
Largest diff. peak and hole	0.245 and −0.276 e SÅ^{-3}

Table 2. Bond lengths (SÅ).

Atoms	Length	Atoms	Length
N1-C5	1.355(3)	C7-O9	1.335(3)
N1-N2	1.377(2)	O9-C10	1.455(2)
N1-C12	1.437(2)	C10-C11	1.477(4)
N2-C3	1.325(2)	C12-C13	1.374(3)
C3-C4	1.397(3)	C12-C17	1.380(3)
C4-C5	1.392(2)	C13-C14	1.389(3)
C4-C7	1.467(3)	C14-C15	1.382(4)
C5-C6	1.484(3)	C15-C16	1.360(3)
C7-O8	1.206(2)	C16-C17	1.387(2)

Table 3. Bond angles (°).

Atoms	Angle	Atoms	Angle
C5-N1-N2	113.73(13)	O8-C7-C4	123.7(2)
C5-N1-C12	128.58(16)	O9-C7-C4	113.34(15)
N2-N1-C12	117.69(16)	C7-O9-C10	116.71(14)
C3-N2-N1	102.92(17)	O9-C10-C11	107.82(17)
N2-C3-C4	112.97(16)	C13-C12-C17	121.08(16)
C5-C4-C3	105.41(16)	C13-C12-N1	120.01(16)
C5-C4-C7	130.21(19)	C17-C12-N1	118.91(15)
C3-C4-C7	124.36(16)	C12-C13-C14	118.8(2)
N1-C5-C4	104.96(17)	C15-C14-C13	120.5(2)
N1-C5-C6	123.61(15)	C16-C15-C14	119.76(18)
C4-C5-C6	131.31(18)	C15-C16-C17	120.8(2)
O8-C7-O9	122.98(19)	C12-C17-C16	119.03(19)

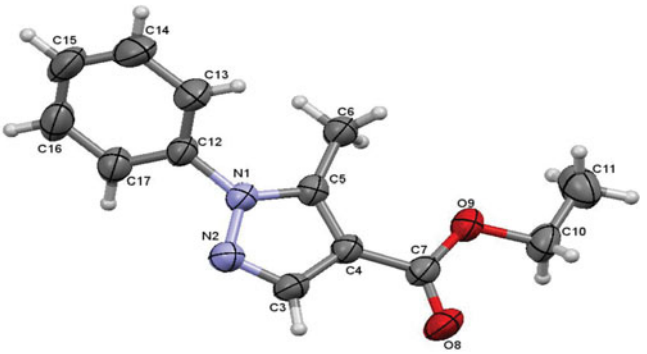

Figure 5. ORTEP of the molecule with thermal ellipsoids drawn at 50% probability.

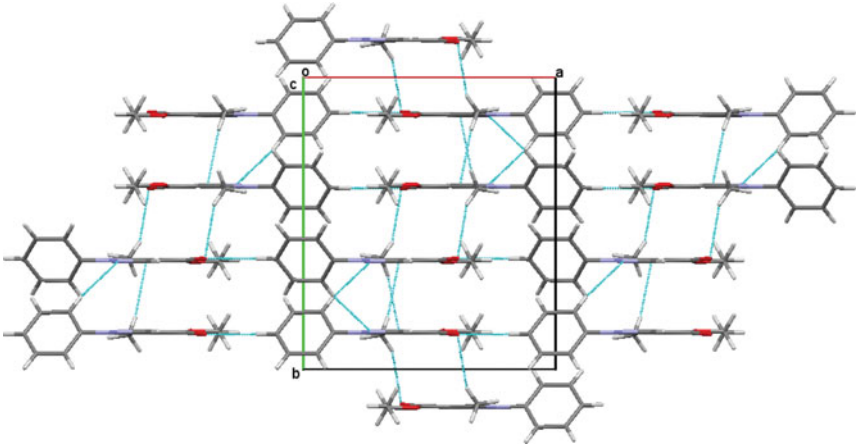

Figure 6. Packing of the molecules when viewed along the *c* axis. The blue dotted lines indicate the C-H$\cdots\pi$ interactions.

respectively, indicates that the ester group lies in the plane of the pyrazole ring and they adopt −antiperiplanar and +antiperiplanar conformations, respectively.

The structure is stabilized by an intermolecular interaction of type C-H···O. The C15-H15···O8 hydrogen bond has a length of 3.457(3) Å and an angle of 177° with the symmetry code $-1+x, y, z$. The crystal structure also involves C-H$\cdots\pi$ interactions and these interactions along with the hydrogen bond links the molecules to form a three dimensional network when viewed along the *c* axis (Fig. 6).

3.6. *Computational studies*

The gas-phase geometry optimization followed by theoretical IR stretching vibrations, and the FMO analysis of the ester molecule was calculated by DFT at the PBE/TZ2P level of theory.

Table 4. Optimized calculations of total energy (a.u.), zero point vibrational energy (eV), entropy (cal/mol-K), dipole moment (Debye), and HOMO-LUMO energy gap (eV) for the ester molecule at PBE/TZ2P basis.

Parameter	PBE/TZ2P
Total energy	−7.28042025
Zero point energy	6.611758
Entropy:	
Total	130.174
Translational	42.202
Vibrational	54.862
Rotational	33.109
Dipole moment	4.6
HOMO-LUMO energy gap	4.01

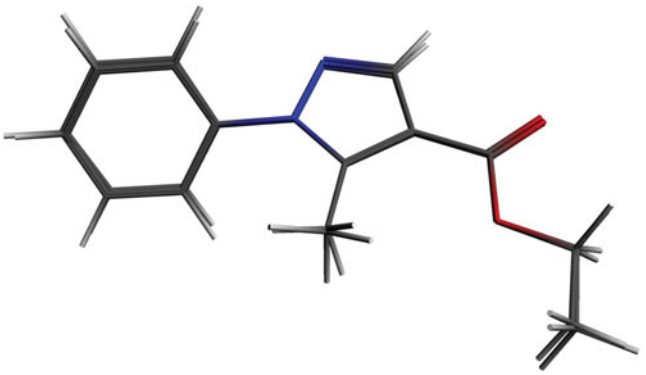

Figure 7. Superposition of the molecular structure obtained from the X-ray diffraction experiment and DFT calculation (PBE/TZ2P).

The calculated total energy, HOMO-LUMO energy gap, and entropy components are given in Table 4. A superposition of the molecular conformations of the ester as established by the DFT calculations and X-ray diffraction study is shown in Fig. 7. It was observed that the two structures resemble each other very closely with small deviations for protons and C = O group. The structural deviation of the molecule in different physical state could attribute largely to the observed discrepancies between the experimental and the calculated properties. However, these systematic errors can be ignored while attempting the structural assignments of the molecule under study.

The pictorial representations of the FMOs of the ester molecule are depicted shown in Fig. 8. The energy gap between the HOMO and the LUMO has been used to qualitative analysis of the stability and reactivity of molecules. The higher HOMO-LUMO gap infers that the molecules are stable and unreactive; while the molecules with small gaps are reactive. The HOMO is mainly localized on the aromatic and pyrazole ring, while the LUMO is delocalized along the whole molecule, indicating that the molecule possesses better intramolecular charge transfer ability. The results indicate the eventual charge transfer interaction taking place within the molecule.

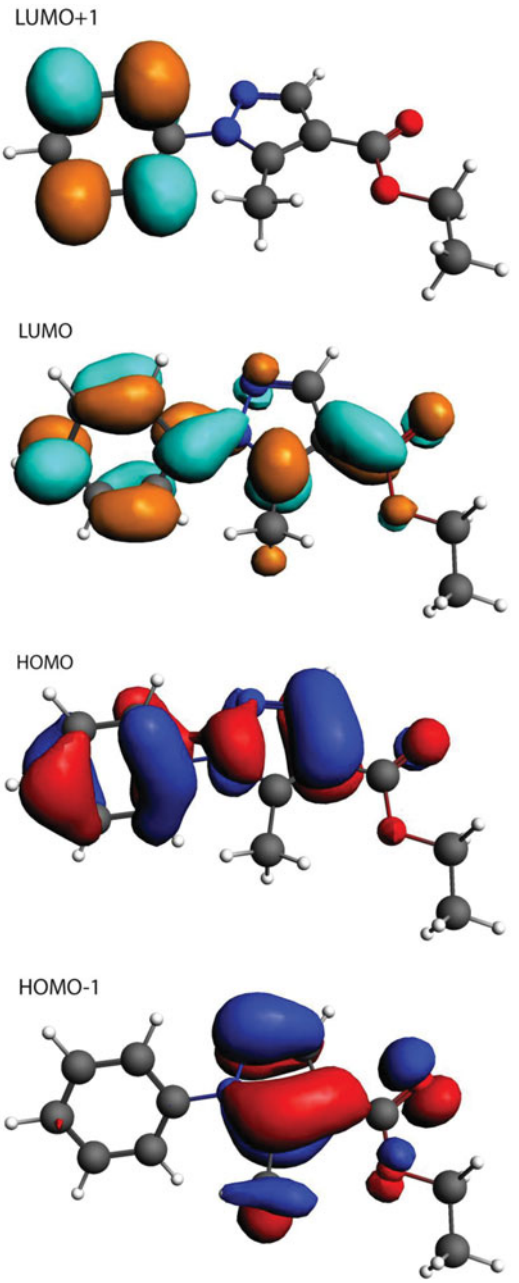

Figure 8. Graphical representations of FMOs.

Conclusions

The present study reports the successful synthesis and isolation of 5-methyl-1-phenyl-1H-4-pyrazolecarboxylate. The UV-Vis spectrum and elemental analysis reveal the excitation properties and composition of the title compound while the TGA and DSC studies have revealed the thermal stability of the crystal. The FTIR spectrum characterizes the presence of functionality of the crystal and ^{1}H NMR identifies the carbon-hydrogen framework, thus helping to solve the solution structure of the molecule. The crystal structure of the title compound reveals that the molecule is nonplanar and the structure is stabilized by an intermolecular

hydrogen bond of the type C-H···O and the structure also involves C-H···π interactions. DFT calculations compliment the experimental results. All the theoretical parameters are in good agreement with the X-ray powder diffraction values.

Acknowledgments

The authors are grateful to the Institution of Excellence, Vijnana Bhavana, University of Mysore, India, for providing the single-crystal X-ray diffractometer facility. The authors gratefully acknowledge the DST-PURSE for the financial assistance. Authors thank Mangalore University for the instrumental facilities.

References

[1] Selvam, C., Jachak, S. M., Thilagavathi, R., & Chakraborti, A. K. (2005). *Bioorg. Med. Chem. Lett.*, *15*, 1793.
[2] Viveka, S., Dinesha, Madhu, L. N., & Nagaraja, G. K. (2015). *Monatsh. Chem. Mon.* (Accepted DOI: 10.1007/s00706–015–1428–5).
[3] Daidone, G. et al. (1998). *Eur. J. Med. Chem*., *33*, 375–382.
[4] Hsu, T. C., Robins, R. K., & Cheng, C. C. (1956). *Science*, *13*, 848.
[5] Genin, M. J. et al. (2000). *J. Med. Chem*., *43*, 1034.
[6] Morimoto, K. M., Makino, K., Yamamoto, S., & Sakato, G. J. (1990). *J. Heterocycl. Chem.*, *27*, 807.
[7] Naoto, M. et al. (1990). *Eur. Pat. Appl. EP.*, *361827*, 120.
[8] Kumar, A. et al. (2003). *Indian J. Chem*., *42B*, 1979.
[9] Navarrete-Vazquez, G. et al. (2003). *Bioorg. Med. Chem*., *11*, 4615.
[10] Ancheta, P. B. et al. (2004). *Vet. Parasitol.*, *120*, 107.
[11] Fustero, S., Sánchez-Roselló, M., Barrio, P., & Simón-Fuentes, A. (2011). *Chem. Rev.*, *111*, 6984.
[12] Chou, L. C. et al. (2007). *Bioorg. Med. Chem*., *15*, 1732.
[13] Pinto, D. J. P. et al. (2007). *J. Med. Chem*., *50*, 5339.
[14] Viveka, S., Prabhuswamy, M., Dinesha, Lokanath, N. K., & Nagaraja, G. K. (2014). *Mol. Cryst. Liq. Cryst.*, *588*, 83.
[15] Viveka, S., Prabhuswamy, M., Dinesha, Lokanath, N. K., & Nagaraja, G. K. (2014). *Mol. Cryst. Liq. Cryst.*, *593*, 261.
[16] Neese, F. (2009). *Coord. Chem. Rev.*, *253*, 526.
[17] Qasim, M. et al. (2007). *Chemosphere*, *69*, 1144–1150.
[18] Bruker. (2012). *SAINT PLUS*, Bruker AXS Inc., Madison, Wisconsin, USA.
[19] Te Velde, G. et al. (2001). Chemistry with ADF, *J. Comput. Chem*., *22*, 931
[20] GUI (2014). SCM, Amsterdam, The Netherlands, http:\\www.scm.com
[21] Perdew, J. P., Burke, K., & Ernzerhof, M. (1996). *Phys. Rev. Lett.*, *77*, 3865.
[22] Reddy, C. S., Rao, L. S., Kumar, G. R., & Nagaraj, A. (2010). *Chem. Pharm. Bull.*, *58*, 1328.
[23] Sheldrick, G. M. (2008). *Acta. Cryst*., *A64*, 112.
[24] Spek, A. L. (1990). *Acta. Cryst*., *A46*, C34.
[25] Macrae, C. F. et al. (2008). *J. Appl. Cryst.*, *41*, 466.